Available online at www.sciencedirect.com

SciVerse ScienceDirect

Procedia IUTAM 3 (2012) 314 – 330

Procedia IUTAM

www.elsevier.com/locate/procedia

Linking Scales in Computations: from Microstructure to Macro-scale Properties

Modeling microstructural effects in dilatational plasticity of polycrystalline materials

Ricardo A. Lebensohn[a]*, Martin I. Idiart[b,c], Pedro Ponte Castañeda[d,e]

[a] *Materials Science and Technology Division, Los Alamos National Laboratory, MS G755, Los Alamos, NM 87845, USA.*
[b] *Departamento de Aeronáutica, Facultad de Ingeniería, Universidad Nacional de La Plata, Calles 1 y 47, La Plata B1900TAG, Argentina.*
[c] *Consejo Nacional de Investigaciones Científicas y Técnicas (CONICET), CCT La Plata, Calle 8 N°1467 , La Plata B1904CMC, Argentina.*
[d] *Department of Mechanical Engineering and Applied Mechanics,University of Pennsylvania, Philadelphia, PA 19104-6315, USA*
[e] *IMDEA Materials Institute, Madrid, E-28040, Spain.*

Elsevier use only: Received date here; revised date here; accepted date here

Abstract

In a recent paper [1] we presented a new constitutive model for the viscoplastic response of polycrystalline aggregates accounting for local anisotropy induced by crystal plasticity and dilatational effects associated with the presence of intergranular cavities. In this contribution we provide a summary of our findings, as well as previously unpublished details of the numerical algorithm underlying this novel formulation. The formulation is based on homogenization and captures microstructural effects on the dilatational plastic behavior of polycrystalline materials. These effects are relevant to many engineering problems in which the presence of cavities embedded in a heterogeneous and anisotropic polycrystalline matrix must be accounted for, and for which standard polycrystalline models of incompressible plasticity, or dilatational plasticity formulations for voided materials with uniform properties of the matrix, have been proven to be insufficient. The present approach makes use of variational linear-comparison homogenization methods to develop constitutive models simultaneously accounting for texture of the matrix, porosity and average pore shape and orientation. The predictions of the models are compared with full-field numerical simulations based on fast Fourier transforms to study the influence of different microstructural features (e.g. overall porosity, single-crystal anisotropy, etc.) and triaxiality on the dilatational viscoplastic behavior of voided fcc polycrystals.

Keywords: polycrystals, porous materials, dilatational plasticity, homogenization, microstructural effects

* Corresponding author. Tel.: +1-505-665-3035
E-mail address: lebenso@lanl.gov.

 doi:10.1016/j.piutam.2012.03.020

1. Introduction

In a recent paper [1] we presented a new constitutive model for the viscoplastic response of polycrystalline aggregates accounting for local anisotropy induced by crystal plasticity and dilatational effects associated with the presence of intergranular cavities. In this contribution we provide a summary of our findings, as well as previously unpublished details of the numerical algorithms underlying this novel formulation.

A formulation based on homogenization, able to capture microstructural effects on dilatational plastic behavior of polycrystalline materials is relevant to many engineering problems in which microstructural effects associated with the presence of cavities embedded in a heterogeneous and anisotropic matrix must be accounted for, and for which standard polycrystalline models of incompressible plasticity, or dilatational plasticity formulations for voided materials with uniform properties of the matrix are not sufficient.

Until our recent work [1], most available theories of dilatational viscoplasticity made use of the simplifying assumption of homogeneity of the material surrounding the cavities, and, therefore, were unable to capture the effect of the strong spatial variations of material properties in the polycrystalline matrix. The widely-used Gurson theory [2] and its various generalizations (e.g. [3-8]) are based on approximate solutions of a hollow sphere (or ellipsoid) with uniform material properties. In contrast, the new dilatational viscoplasticity theory for polycrystalline voided solids [1] accounts for the heterogeneity associated with both the crystallites and the cavities, on an equal footing.

Several constitutive theories were available to estimate the viscoplastic response of fully dense polycrystalline solids in terms of their morphological and crystallographic texture. For linearly viscous polycrystals, the so-called self-consistent (SC) theory has been found to be both very accurate [9-10] and easy-to-use. Driven by the need to understand plastic deformation in metals and other polycrystalline solids, many attempts have been made to generalize the SC formulation to nonlinear constitutive responses. Classical first-order nonlinear SC theories (e.g.[11-15]) made use of the linear SC solution, together with a linearization scheme to approximate the grain interactions. However, while these theories generally provide improvements over the Taylor and Sachs approximations, they are known to give unphysical predictions for voided solids [15]. The reason for this is that their linearization schemes are based on the first moments of the fields only, while the presence of cavities induces strong field gradients in the solid phases, making it necessary to use linearization schemes containing also higher-order information on the field distributions.

Improved nonlinear SC theories are available from the work of Ponte Castañeda and co-workers [16-25]. These theories rely on the use of a "linear-comparison polycrystal" (LCP), consisting of a polycrystal with the same microstructure as the nonlinear polycrystal but whose single crystal response is identified with a certain linearization of the corresponding nonlinear response, typically guided by suitably-designed variational principles. The difference between the various LCP theories lies on the choice of the linearization scheme. In particular, Liu and Ponte Castaneda [25] proposed a second-order theory that makes use of a "generalized-secant" (GSEC) interpolation of the nonlinear local response [24], incorporating dependence on both the first and second moments of the fields and preserving the exactness to second-order in the contrast. Dilatational viscoplasticity models for polycrystalline voided solids were derived in [1] by extending this GSEC theory. The resulting model was able to account for morphological and crystallographic texture of the polycrystalline matrix, as well as porosity and average pore shape and orientation.

The proposed SC model is also compared here with full-field numerical simulations, carried out using a fast Fourier transform (FFT)-based method. This method, which provides the exact solution of the governing equations in a periodic medium, was originally developed by Suquet and co-workers [26-27] as a fast algorithm to compute the elastic and elastoplastic effective and local response of composites, and later adapted by Lebensohn and co-workers [9-10, 28-30] to deal with the viscoplastic deformation of power-law polycrystals, including voided polycrystals [1]. Results of FFT-based full-field simulations and the mean-field SC models are here compared to assess the effect of crystallinity, crystallographic texture and porosity in porous fcc polycrystals.

2. Mean-field approach

In what follows, a voided polycrystal is represented by a set of N_r weighted, ellipsoidal, statistically representative (SR) grains and voids. Each SR grain represents the average behavior of all grains with a particular crystallographic orientation and a given morphology, but different environments deforming in a viscoplastic

(incompressible) regime. Each SR void represents the average behavior of all voids with a particular morphology, but different environments. These SR grains and voids should be regarded as representing the behavior of *mechanical phases*, i.e. all single-crystal grains with a given orientation and the same morphology belong to mechanical phase (g) and are represented by SR grain (g), and all voids of the same morphology belong to mechanical phase (v) and are represented by SR void (v). The voids are treated on the same footing as grains, which corresponds to the problem of a polycrystal with intergranular voids. The effective behavior of such aggregate turns out to be sensitive to the hydrostatic stress component and to exhibit a dilatational strain rate component. Locally, the grains deform by crystal plasticity mechanisms: i.e. slip systems activated by a resolved shear stress, giving raise to incompressible deformation. Meanwhile, voids are able to change shape and volume, but cannot sustain stress.

2.1. Local constitutive behavior and polycrystal model

The incompressible viscoplastic constitutive behavior of a material point **x** belonging to a single-crystal grain is described by means of the following non-linear, rate-sensitive equation relating the stress **σ** and the strain rate **ε** at point **x**:

$$\dot{\boldsymbol{\varepsilon}}(\mathbf{x}) = \dot{\gamma}_o \sum_{k=1}^{N_k} \mathbf{m}^k(\mathbf{x}) \left(\frac{\left| \mathbf{m}^k(\mathbf{x}) : \boldsymbol{\sigma}(\mathbf{x}) \right|}{\tau_o^k(\mathbf{x})} \right)^n \operatorname{sgn}\left(\mathbf{m}^k(\mathbf{x}) : \boldsymbol{\sigma}(\mathbf{x}) \right) \tag{1}$$

where $\tau_o^k(\mathbf{x})$ and $\mathbf{m}^k(\mathbf{x})$ are, respectively, the critical resolved shear stress (CRSS) and the Schmid tensor, associated with each slip system *k* of the N_k systems available, $\dot{\gamma}_o$ is a normalization factor, and *n* is the stress exponent. The latter constitutive equation derives from a single-crystal stress potential defined as:

$$u(\mathbf{x}, \boldsymbol{\sigma}) = \sum_{k=1}^{N_k} \frac{\dot{\gamma}_o \tau_o^k(\mathbf{x})}{n+1} \left(\frac{\left| m^k(\mathbf{x}) : \boldsymbol{\sigma}(\mathbf{x}) \right|}{\tau_o^k(\mathbf{x})} \right)^{n+1} \tag{2}$$

such that: $\dot{\varepsilon}(\mathbf{x}) = \partial u(\mathbf{x}, \boldsymbol{\sigma}) / \partial \boldsymbol{\sigma}$. Considering the characteristic functions of N_r SR grains and one SR void (phase "0"): $\chi^{(r)}(\mathbf{x})$, r = 0, N_r , which take the value 1 if **x** belong to mechanical phase (r) and 0 otherwise, one can write:

$$u(\mathbf{x}, \boldsymbol{\sigma}) = \sum_{r=0}^{N_r} \chi^{(r)}(\mathbf{x})\, u^{(r)}(\boldsymbol{\sigma}) \tag{3}$$

where the stress potential of the single SR void: $u^{(0)}(\boldsymbol{\sigma}) = 0$ if $\boldsymbol{\sigma} = 0$ and infinity otherwise, and the stress potentials of the grains are given by:

$$u^{(r)}(\boldsymbol{\sigma}) = \sum_{k=1}^{N_k} \phi^{k(r)}\left(\tau^{k(r)} \right) \tag{4}$$

with r = 1, N_r , where the resolved stress is given by $\tau^{k(r)} = \mathbf{m}^{k(r)} : \boldsymbol{\sigma}$, and:

$$\phi^{k(r)}(\tau^{k(r)}) = \frac{\dot{\gamma}_o \tau_o^k(\mathbf{x})}{n+1} \left(\frac{\left| \tau^{k(r)} \right|}{\tau_o^k(\mathbf{x})} \right)^{n+1} \tag{5}$$

The weights (volume fractions) associated with the SR grains and void are $c^{(r)} = <\chi^{(r)}(\mathbf{x})>$, where <.> denotes volume average. The porosity of the aggregate is given by $f = c^{(0)}$, with which we can define a set of re-normalized weights as: $c_g^{(r)} = c^{(r)}/(1-f)$.

Due to the microstructural inhomogeneity, the local fields $\dot{\boldsymbol{\varepsilon}}(\mathbf{x})$ and $\boldsymbol{\sigma}(\mathbf{x})$ exhibit strong spatial variations within the aggregate. The effective viscoplastic behavior of the aggregate is defined as the relation between the average stress $\boldsymbol{\Sigma} = <\boldsymbol{\sigma}(\mathbf{x})>$ and the average strain rate $\dot{\mathbf{E}} = <\dot{\boldsymbol{\varepsilon}}(\mathbf{x})>$ over the aggregate. Formally, it can be characterized by:

$$\dot{\mathbf{E}} = \frac{\partial \tilde{u}}{\partial \boldsymbol{\Sigma}}(\boldsymbol{\Sigma}); \quad \tilde{u}(\boldsymbol{\Sigma}) = \min_{\boldsymbol{\sigma} \in S(\boldsymbol{\Sigma})} \left\langle u(\mathbf{x}, \boldsymbol{\sigma}) \right\rangle = (1-f) \min_{\boldsymbol{\sigma} \in S^*(\boldsymbol{\Sigma})} \sum_{r=1}^{N_r} c_g^{(r)} \left\langle u^{(r)}(\boldsymbol{\sigma}) \right\rangle^{(r)} \tag{6}$$

where $\tilde{u}(\boldsymbol{\Sigma})$ is the effective stress potential for the aggregate. In this definition, $S(\boldsymbol{\Sigma})$ denotes the set of statically-admissible stress fields with prescribed average $\boldsymbol{\Sigma}$, while $S^*(\boldsymbol{\Sigma})$ is the subset of the latter with zero traction vector on the surface of the cavities. Carrying out this minimization is in general an intractable problem. In what follows, we will generate approximate estimates for the effective potential by means of variational linear-comparison methods. Corresponding estimates for the effective behavior of the aggregate may then be generated by differentiation, according to relation $(6)_1$.

2.2. Linear self-consistent estimates

In this section we first recall the self-consistent solution for *fully-dense* linear polycrystals and then present the extension to the case of *porous* linear aggregates. A fully-dense thermoelastic linear-comparison polycrystal is defined by local stress-strain-rate relations of the form:

$$\dot{\boldsymbol{\varepsilon}} = \mathbf{M}^{(r)} : \boldsymbol{\sigma} + \dot{\mathbf{e}}^{(r)} \tag{7}$$

where $\mathbf{M}^{(r)}$ and $\dot{\mathbf{e}}^{(r)}$ are viscous compliance and back-extrapolated strain rate tensors of each mechanical phase (r), respectively. The associated stress potentials can be written as:

$$u_L^{(r)}(\boldsymbol{\sigma}) = \frac{1}{2}\boldsymbol{\sigma} : \mathbf{M}^{(r)} : \boldsymbol{\sigma} + \dot{\mathbf{e}}^{(r)} : \boldsymbol{\sigma} \tag{8}$$

and the corresponding effective stress potential is given by:

$$\tilde{u}_L(\boldsymbol{\Sigma}) = \min_{\boldsymbol{\sigma} \in S(\boldsymbol{\Sigma})} \sum_{r=1}^{N_r} c^{(r)} \left\langle u_L^{(r)}(\boldsymbol{\sigma}) \right\rangle^{(r)} \tag{9}$$

When local stress potentials are given by Eq. (8), the corresponding effective stress potential (Eq. 9) may be written in the form [31,32]:

$$\tilde{u}_L(\boldsymbol{\Sigma}) = \frac{1}{2}\boldsymbol{\Sigma} : \tilde{\mathbf{M}} : \boldsymbol{\Sigma} + \tilde{\mathbf{e}} : \boldsymbol{\Sigma} + \frac{1}{2}\tilde{g} \tag{10}$$

and the overall moduli can be calculated self-consistently as [31-33]:

$$\tilde{\mathbf{M}} = \sum_{r=1}^{N_r} c^{(r)} \mathbf{M}^{(r)} : \mathbf{B}^{(r)} \tag{11}$$

$$\tilde{\dot{\mathbf{e}}} = \sum_{r=1}^{N_r} c^{(r)} \mathbf{B}^{(r)T} \cdot \dot{\mathbf{e}}^{(r)} \tag{12}$$

$$\tilde{g} = \sum_{r=1}^{N_r} c^{(r)} \mathbf{b}^{(r)} \cdot \dot{\mathbf{e}}^{(r)} \tag{13}$$

In these expressions the *localization tensors* are given by:

$$\mathbf{B}^{(r)} = \left(\mathbf{M}^{(r)} + \tilde{\mathbf{M}}^*\right)^{-1} : \left(\tilde{\mathbf{M}} + \tilde{\mathbf{M}}^*\right) \tag{14}$$

$$\mathbf{b}^{(r)} = \left(\mathbf{M}^{(r)} + \tilde{\mathbf{M}}^*\right)^{-1} : \left(\tilde{\dot{\mathbf{e}}} - \dot{\mathbf{e}}^{(r)}\right) \tag{15}$$

where $\tilde{\mathbf{M}}^*$ is the *interaction tensor* that depends on $\tilde{\mathbf{M}}$ and the "shape" of the two-point correlation functions for the distribution of the grain orientations and the porosity within the aggregate, such that:

$$\tilde{\mathbf{M}}^* = \left(\mathbf{I} - \mathbf{S}\right)^{-1} : \mathbf{S} : \tilde{\mathbf{M}} \tag{16}$$

where $\mathbf{S}$ is the *Eshelby tensor* (e.g. see [33] for numerical details).

In the case of a voided thermoelastic linear-comparison polycrystal, we have: $\left(\mathbf{M}^{(0)}\right)^{-1} = 0$ and $\dot{\mathbf{e}}^{(0)} = 0$ for the void phase (c.f. Eq. 7) and the effective stress potential (c.f. Eq. 9) is given by:

$$\tilde{u}_L(\boldsymbol{\Sigma}) = \left(1 - f\right) \min_{\boldsymbol{\sigma} \in S^*(\boldsymbol{\Sigma})} \sum_{r=1}^{N_r} c_g^{(r)} \left\langle u_L^{(r)}(\boldsymbol{\sigma}) \right\rangle^{(r)} \tag{17}$$

Moreover, the localization tensors in the void phase are:

$$\mathbf{B}^{(0)} = \mathbf{b}^{(0)} = 0 \tag{18}$$

With this, and considering the following limit:

$$\lim_{\mathbf{M}^{(0)} \to \infty} \mathbf{M}^{(0)} : \mathbf{B}^{(0)} = \lim_{\mathbf{M}^{(0)} \to \infty} \mathbf{M}^{(0)} : \left(\mathbf{M}^{(0)} + \tilde{\mathbf{M}}^*\right)^{-1} : \left(\tilde{\mathbf{M}} + \tilde{\mathbf{M}}^*\right) = \tilde{\mathbf{M}} + \tilde{\mathbf{M}}^* \tag{19}$$

the self-consistent relations (11-13) for the voided polycrystal become [1]:

$$\tilde{\mathbf{M}} = \sum_{r=1}^{N_r} c_g^{(r)} \mathbf{M}^{(r)} : \mathbf{B}^{(r)} + \frac{f}{1-f} \tilde{\mathbf{M}}^* \tag{20}$$

$$\tilde{\dot{\mathbf{e}}} = \left(1 - f\right) \sum_{r=1}^{N_r} c_g^{(r)} \mathbf{B}^{(r)T} \cdot \dot{\mathbf{e}}^{(r)} \tag{21}$$

$$\tilde{g} = \left(1 - f\right) \sum_{r=1}^{N_r} c_g^{(r)} \mathbf{b}^{(r)} \cdot \dot{\mathbf{e}}^{(r)} \tag{22}$$

The associated estimate for the effective stress–strain-rate relation follows from differentiation of (9), and is given by:

$$\dot{\mathbf{E}} = \tilde{\mathbf{M}} : \boldsymbol{\Sigma} + \tilde{\dot{\mathbf{e}}} \tag{23}$$

In turn, corresponding estimates for the first and second moments of the stress field in each solid phase (r), required by the linear-comparison theories (see below), are given by:

$$\overline{\boldsymbol{\sigma}}^{(r)} = \mathbf{B}^{(r)} : \boldsymbol{\Sigma} + \mathbf{b}^{(r)} \tag{24}$$

$$\left\langle \boldsymbol{\sigma} \otimes \boldsymbol{\sigma} \right\rangle^{(r)} = \frac{1}{1-f} \frac{2}{c_g^{(r)}} \frac{\partial \tilde{u}_L}{\partial \mathbf{M}^{(r)}} \tag{25}$$

The algorithm to calculate the latter is given in the Appendix. With them, the second moment of the intraphase stress fluctuations is given by:

$$\mathbf{C}_{\sigma}^{(r)} = \left\langle \left(\boldsymbol{\sigma} - \overline{\boldsymbol{\sigma}}^{(r)} \right) \otimes \left(\boldsymbol{\sigma} - \overline{\boldsymbol{\sigma}}^{(r)} \right) \right\rangle^{(r)} = \left\langle \boldsymbol{\sigma} \otimes \boldsymbol{\sigma} \right\rangle^{(r)} - \overline{\boldsymbol{\sigma}}^{(r)} \otimes \overline{\boldsymbol{\sigma}}^{(r)} \tag{26}$$

2.3. Nonlinear self-consistent estimates

Estimates for the effective potential of nonlinear voided polycrystals are generated here by means of the GSEC variational theory of Liu and Ponte Castaneda [25]. This second-order theory was originally derived for the case of fully-dense polycrystals under the assumption of incompressible constituent phases. In this section we present the extention of the theory to account for the presence of a compressible voided phase [1]. The theory makes use of a linear-comparison voided polycrystal with the same microstructure as the nonlinear polycrystal but with local stress potentials given by Eq. (8), where:

$$\mathbf{M}^{(r)} = \sum_{k=1}^{N_k} \alpha^{k(r)} \left(\mathbf{m}^{k(r)} \otimes \mathbf{m}^{k(r)} \right) \tag{27}$$

$$\dot{\mathbf{e}}^{(r)} = \sum_{k=1}^{N_k} \dot{e}^{k(r)} \mathbf{m}^{k(r)} \tag{28}$$

define the viscous-compliance and back-extrapolated strain rate tensors at crystal level $\left(r = 1, N_r\right)$, in terms of the corresponding slip-level quantities $\alpha^{k(r)}$ and $\dot{e}^{k(r)}$, respectively. The local potentials of the nonlinear polycrystal are then approximated in terms of the local potentials of the linear-comparison polycrystal, and a suitable measure of the error, to obtain the following approximation for the effective potential of the nonlinear polycrystal:

$$\tilde{u}(\boldsymbol{\Sigma}) = \left(1-f\right) \sum_{r=1}^{N_r} \sum_{k=1}^{N_k} c_g^{(r)} \left[\phi^{k(r)} \left(\hat{\tau}^{k(r)} \right) - \phi'^{k(r)} \left(\overline{\tau}^{k(r)} \right) \left(\hat{\tau}^{k(r)} - \overline{\tau}^{k(r)} \right) \right] \tag{29}$$

In this expression, the variables $\overline{\tau}^{k(r)}$ and $\hat{\tau}^{k(r)}$ depend on the averages and fluctuations of the resolved shear stresses in the linear-comparison polycrystal:

$$\overline{\tau}^{k(r)} = \left\langle \mathbf{m}^{k(r)} : \boldsymbol{\sigma} \right\rangle^{(r)} = \mathbf{m}^{k(r)} : \overline{\boldsymbol{\sigma}}^{(r)} \tag{30}$$

$$\left(\hat{\tau}^{k(r)} - \overline{\tau}^{k(r)} \right)^2 = \left\langle \left(\mathbf{m}^{k(r)} : \boldsymbol{\sigma} - \overline{\tau}^{k(r)} \right)^2 \right\rangle^{(r)} = \mathbf{m}^{k(r)} : \mathbf{C}_{\sigma}^{(r)} : \mathbf{m}^{k(r)} \tag{31}$$

where the quantities $\hat{\tau}^{k(r)} - \bar{\tau}^{k(r)}$ are taken to have the same sign as $\bar{\tau}^{k(r)}$. Self-consistent estimates for $\bar{\boldsymbol{\sigma}}^{(r)}$ and $\mathbf{C}_{\sigma}^{(r)}$ are given by Eqs. (24) and (26), respectively. In turn, the properties of the LCP must be specified such that the magnitudes in Eqs. (27-28) satisfy the relations:

$$\dot{e}^{k(r)} = \phi'^{k(r)}\left(\bar{\tau}^{k(r)}\right) - \alpha^{k(r)}\bar{\tau}^{k(r)} \tag{32}$$

$$\phi'^{k(r)}\left(\hat{\tau}^{k(r)}\right) - \phi'^{k(r)}\left(\bar{\tau}^{k(r)}\right) = \alpha^{k(r)}\left(\hat{\tau}^{k(r)} - \bar{\tau}^{k(r)}\right) \tag{33}$$

Equations (30-33) together with (24-26) constitute a system of nonlinear algebraic equations for the variables $\dot{e}^{k(r)}$ and $\alpha^{k(r)}$, which must be solved numerically, in general. The solution of these equations and GSEC linearization scheme were implemented in the ViscoPlastic Self-Consistent (VPSC) code [14], suitably modified to account for the presence of a compressible voided phase [34]. Finally, an estimate for the effective behavior of the polycrystal can be obtained by differentiating Eq. (29) with respect to $\boldsymbol{\Sigma}$:

$$\dot{\mathbf{E}} = \dot{\mathbf{E}}_L - (1-f)\sum_{r=1}^{N_r}\sum_{k=1}^{N_k} c_g^{(r)}\left[\phi''^{k(r)}\left(\bar{\tau}^{k(r)}\right) - \alpha^{k(r)}\right]\left(\hat{\tau}^{k(r)} - \bar{\tau}^{k(r)}\right)\frac{\partial \bar{\tau}^{k(r)}}{\partial \boldsymbol{\Sigma}} \tag{34}$$

where $\dot{\mathbf{E}}_L$ is is the macroscopic strain rate in the LCP, which is given in terms of the linear properties (27-28) by an expression of the form (23), and can be shown to reduce to:

$$\dot{\mathbf{E}}_L = (1-f)\sum_{r=1}^{N_r}\sum_{k=1}^{N_k} c_g^{(r)}\mathbf{m}^{k(r)}\phi'^{k(r)}\left(\bar{\tau}^{k(r)}\right) + f\left(\tilde{\mathbf{M}} + \tilde{\mathbf{M}}^*\right):\boldsymbol{\Sigma} \tag{35}$$

The stress–strain-rate relation (34) does not coincide exactly with the effective stress–strain-rate relation for the underlying linear-comparison polycrystal. It contains additional terms that depend on the derivatives of the average shear stresses which must be determined by differentiating Eqs. (30-33). An alternative approach for the estimation of the stress–strain-rate relation consists in the direct use Eq. (35) or the linear-comparison polycrystal. While this avoids the need to compute the aforementioned derivatives, it should be emphasized that relation (35) does not possess an associated potential function and is not exact to second order in the heterogeneity contrast. It can be interpreted as a generalization of the so-called affine approximation of Masson et al. [15], including the effect of field fluctuations (see [24] for more details).

3. Full-field Model

The FFT-based full-field formulation for viscoplastic polycrystals is conceived for periodic unit cells, provides an exact solution of the governing equations. It was originally developed [27,28] as a fast algorithm to compute the elastic and elastoplastic effective and local response of composites, and later adapted [28-30] to deal with the viscoplastic deformation of power-law solid (incompressible) polycrystals.

In what follows, we describe the FFT-based method to the case of viscoplasticity of polycrystals with voids [1]. Moreover, since one of our goals is to assess the effect of crystallinity on the dilatational viscoplastic behavior of porous materials, we will also address the FFT-based solution for voided materials with nonlinear isotropic matrix.

3.1. Unit cell construction

The granular microstructures considered here are periodic unit cells generated by Voronoi tessellation, with intergranular cavities. 200 grain nuclei were randomly distributed in cubic domain, and, to ensure periodicity of the microstructure, they were periodically duplicated immediately outside the unit cube. The sides of the unit cell were partitioned, determining a N_1x N_2x N_3 regular Fourier grid. Each Fourier point was assigned to its nearest nucleus.

All the Fourier points at multiple junctions were identified and picked in a random sequence to try to accommodate a cavity of a radius r_1, surrounded by a "security" zone of radius r_2 ($> r_1$) where no other cavity was allowed.

In order to assess the role of crystallinity on the dilatational viscoplastic response of porous materials, the above unit cell has in turn been modified to represent a voided material consisting of a nonlinear isotropic matrix having the same porosity and distribution of cavities as the voided polycrystal. For this, the Fourier points belonging to grains, were assigned to a solid nonlinear isotropic phase, with the same stress exponent and a flow stress equal to the effective stress calculated (in an additional simulation) for the solid polycrystal.

The discretization of the periodic unit cell representing a porous polycrystal determines a regular grid in the Cartesian space **{x}** and a corresponding grid of the same size in Fourier space **{k}**. A stress is imposed to the unit cell. The local strain rate field is a function of the local velocity field, and can be split into its average and a fluctuation term:

$$\dot{\varepsilon}_{ij}(\mathbf{v}(\mathbf{x})) = \dot{E}_{ij} + \tilde{\dot{\varepsilon}}_{ij}(\tilde{\mathbf{v}}(\mathbf{x})) \tag{36}$$

where:

$$v_i(\mathbf{x}) = \dot{E}_{ij} x_j + \tilde{v}_i(\mathbf{x}) = V_i(\mathbf{x}) + \tilde{v}_i(\mathbf{x}) \tag{37}$$

The local constitutive relation between the strain rate and the stress for material points (i.e. belonging to grains) is given by the rate-sensitivity relation (Eq. 1). Note that the strain rate in material points has no dilatational component. As for the Fourier points belonging to voids, the stress vanishes and the strain rate is non-traceless in general and needs to be determined. Let us choose a fourth-order tensor $\mathbf{L}^o$ to be the stiffness of a linear reference medium, and define the polarization field as:

$$\varphi_{ij}(\mathbf{x}) = \tilde{\sigma}_{ij}(\mathbf{x}) - L^o_{ijkl}\,\tilde{\dot{\varepsilon}}_{kl}(\mathbf{x}) \tag{38}$$

Then, the stress deviation can be written as:

$$\tilde{\sigma}_{ij}(\mathbf{x}) = L^o_{ijkl}\tilde{\dot{\varepsilon}}_{kl}(\mathbf{x}) + \varphi_{ij}(\mathbf{x}) \tag{39}$$

which, combined with the equilibrium condition and $\tilde{\dot{\varepsilon}}_{kl}(\mathbf{x}) = \mathrm{sym}(\tilde{v}_{k,l}(\mathbf{x}))$ gives:

$$L^o_{ijkl}\tilde{v}_{k,lj}(\mathbf{x}) + \varphi_{ij,j}(\mathbf{x}) = 0 \tag{40}$$

The auxiliary differential equation for the Green function of the velocity field is then given by:

$$L^o_{ijkl}\, G_{km,lj}(\mathbf{x}-\mathbf{x}') + \delta_{im}\,\delta(\mathbf{x}-\mathbf{x}') = 0 \tag{41}$$

After some manipulation, the convolution integral that give the velocity deviation field is:

$$\tilde{v}_k(\mathbf{x}) = \int_{R^3} G_{ki,j}(\mathbf{x}-\mathbf{x}')\,\varphi_{ij}(\mathbf{x}')\,d\mathbf{x}' \tag{42}$$

Convolution integrals in direct space are simply products in Fourier space, hence:

$$\hat{\tilde{v}}_k(\mathbf{k}) = (-i\mathbf{k}_j)\,\hat{G}_{ki}(\mathbf{k})\,\hat{\varphi}_{ij}(\mathbf{k}) \tag{43}$$

$$\hat{\tilde{v}}_{i,j}(\mathbf{k}) = \hat{\Gamma}_{ijkl}(\mathbf{k})\,\hat{\varphi}_{kl}(\mathbf{k}) \tag{44}$$

where the symbol "^" indicated a Fourier transform and $\Gamma_{ijkl} = G_{ik,jl}$. The operators in Eqs. (43-44) can be calculated in Fourier space as:

$$\hat{G}_{ij}(\mathbf{k}) = A_{ij}^{-1}(\mathbf{k}), \text{ where: } A_{ik}(\mathbf{k}) = k_l k_j L^o_{ijkl}, \text{ and: } \hat{\Gamma}_{ijkl}(\mathbf{k}) = -k_j k_l \hat{G}_{ik}(\mathbf{k}) \tag{45}$$

3.2. FFT-based Algorithm

The following iterative procedure is based on the augmented Lagrangians algorithm [27] adapted to the case of porous polycrystals, for a stress state imposed to the unit cell. Supraindices indicate values corresponding to the current iteration (e.g. supraindex zero indicates initial guess). The algorithm for a full stress tensor $\boldsymbol{\Sigma}$ imposed to the unit cell needs an initial guess for the average strain rate:

$$\dot{E}^o_{ij} = \dot{E}'^o_{ij} + \frac{\dot{E}^o_{kk}}{3}\delta_{ij} \tag{46}$$

which will be adjusted iteratively. Initial guess values also need to be assigned to the strain rate field in the regular grid:

$$\tilde{\dot{\varepsilon}}'^o_{ij}(\mathbf{x}) = 0 \Rightarrow \dot{\varepsilon}'^o_{ij}(\mathbf{x}) = \dot{E}'_{ij} \qquad (\mathbf{x} \in \text{material and voids}) \tag{47}$$

$$\tilde{\dot{\varepsilon}}^o_{kk}(\mathbf{x}) = -\dot{E}_{kk} \Rightarrow \dot{\varepsilon}^o_{kk}(\mathbf{x}) = 0 \qquad (\mathbf{x} \in \text{material}) \tag{48}$$

$$\tilde{\dot{\varepsilon}}^o_{kk}(\mathbf{x}) = \left(\frac{1}{f} - 1\right)\dot{E}_{kk} \qquad (\mathbf{x} \in \text{voids}) \tag{49}$$

With these initial values, the corresponding stress field in the crystalline material points $\boldsymbol{\sigma}^o(\mathbf{x})$ is obtained inverting the local constitutive relation (Eq. 1). As for the points belonging to voids, the stress simply vanishes. The initial specification of these fields allows us to calculate the initial guess for the polarization field in direct space (Eq. 38), which can be in turn Fourier-transformed. Furthermore, assuming:

$$\lambda^o_{ij}(\mathbf{x}) = \sigma^o_{ij}(\mathbf{x}) \tag{50}$$

as initial guess for a auxiliary stress field associated with the compatibility constraint, the iterative procedure reads as follows. With the polarization field after iteration *i* being known, the *i*+1-th iteration starts by computing the new guess for the kinematically-admissible strain rate fluctuation field:

$$\hat{\tilde{d}}^{i+1}_{ij}(\mathbf{k}) = -\hat{\Gamma}^{sym}_{ijkl}(\mathbf{k})\,\hat{\varphi}^i_{kl}(\mathbf{k}), \quad \forall \mathbf{k} \neq 0; \quad \text{and} \quad \hat{\tilde{d}}^{i+1}_{ij}(\mathbf{0}) = 0 \tag{51}$$

The corresponding field in real space is thus obtained by application of the inverse FFT, and the new guess for the stress field in the grains is calculated from:

$$\boldsymbol{\sigma}^{i+1}(\mathbf{x}) + \mathbf{L}^o : \dot{\boldsymbol{\varepsilon}}^{i+1}(\mathbf{x}) = \boldsymbol{\lambda}^i(\mathbf{x}) + \mathbf{L}^o : \left(\dot{\mathbf{E}}^i + \tilde{\mathbf{d}}^{i+1}(\mathbf{x})\right) \tag{52}$$

which, combined with Eq. (1), gives a 6x6 system of nonlinear algebraic equations to solve for $\boldsymbol{\sigma}^{i+1}(\mathbf{x})$. The iteration is completed with the calculation of new guesses for the Lagrange multiplier field:

$$\boldsymbol{\lambda}^{i+1}(\mathbf{x}) = \boldsymbol{\lambda}^{i}(\mathbf{x}) + L^{o} : \left(\tilde{\boldsymbol{\varepsilon}}^{i+1}(\mathbf{x}) - \tilde{\mathbf{d}}^{i+1}(\mathbf{x})\right) \tag{53}$$

and the new guess for average strain rate [35]:

$$\dot{\mathbf{E}}^{i+1} = \left\langle \dot{\boldsymbol{\varepsilon}}^{i}(\mathbf{x}) \right\rangle + \mathbf{L}^{o^{-1}} : \left(\boldsymbol{\Sigma} - \left\langle \boldsymbol{\sigma}^{i+1}(\mathbf{x}) \right\rangle \right) \tag{54}$$

where <.> indicates average over the entire Fourier grid. The algorithm then advances until the normalized average differences between the stress fields $\boldsymbol{\sigma}(\mathbf{x})$ and $\boldsymbol{\lambda}(\mathbf{x})$ and strain rate fields $\dot{\boldsymbol{\varepsilon}}(\mathbf{x})$ and $\mathbf{d}(\mathbf{x})$ are smaller than a threshold.

For use in the case of porous materials with nonlinear isotropic matrix whose constitutive equation is given by [36]:

$$\dot{\boldsymbol{\varepsilon}}(\mathbf{x}) = \frac{3\dot{\varepsilon}_o}{2\sigma_o}\left(\frac{\sigma_{eq}(\mathbf{x})}{\sigma_o}\right)^{n-1}\boldsymbol{\sigma}(\mathbf{x}) \tag{55}$$

where $\dot{\varepsilon}_o$ is a reference strain-rate and σ_o is the flow stress. The previous algorithm can be followed step by step, replacing the use of Eq. (1) by Eq. (55), as necessary.

4. Results

The methods presented above are used here to study the influence of crystallinity, texture and porosity on the instantaneous response of porous polycrystalline solids. Of particular interest is to assess the simplifying assumption made in most homogenization-type theories of dilatational viscoplasticity that the matrix material surrounding the cavities is homogeneous and isotropic. For this reason, attention is restricted to polycrystalline solids with isotropic morphological statistics, that is, with equiaxed grains with uniformly-distributed crystal orientations and isotropically distributed porosity.

The single-crystal behavior characterized by slip potentials given by Eq. (5) corresponds to fcc crystals deforming plastically by glide on 12 {111}<110> slip systems with $\tau_o^k = \tau_o$, $k = 1,12$, $\dot{\gamma}_o = 1$, and a stress exponent n=10. The fact that the stress exponent and the reference strain rate are the same for all the slip systems and grains in a given polycrystal simplifies the analysis considerably. The local potential $\tilde{u}(\boldsymbol{\sigma})$ is in this case a homogeneous function of degree n+1 in $\boldsymbol{\sigma}$, and consequently, the corresponding effective potential $\tilde{u}(\boldsymbol{\Sigma})$ is a homogeneous function of degree n+1 in $\boldsymbol{\Sigma}$ [36]. Then, a single equipotential surface $\tilde{u}(\boldsymbol{\Sigma}) = \text{constant}$ fully characterizes $\tilde{u}$; any other equipotential surface is simply a homothetic surface [3]. Results for power-law polycrystals are reported here in the form of equipotential surfaces given by:

$$\left\{ \boldsymbol{\Sigma}^* : \tilde{u}(\boldsymbol{\Sigma}^*) = \frac{\sigma_o^{-n}\dot{\gamma}_o}{n+1} \right\} \tag{56}$$

where σ_o is some reference flow stress, see below. This is the so-called gauge surface of the polycrystal, which characterizes completely the effective response [3]. A more convenient equation for the gauge surface can be obtained by writing the effective potential as:

$$\tilde{u}(\boldsymbol{\Sigma}) = \frac{\sigma_o\dot{\gamma}_o}{n+1}\left(\frac{\Lambda(\boldsymbol{\Sigma})}{\sigma_o}\right)^{n+1} \tag{57}$$

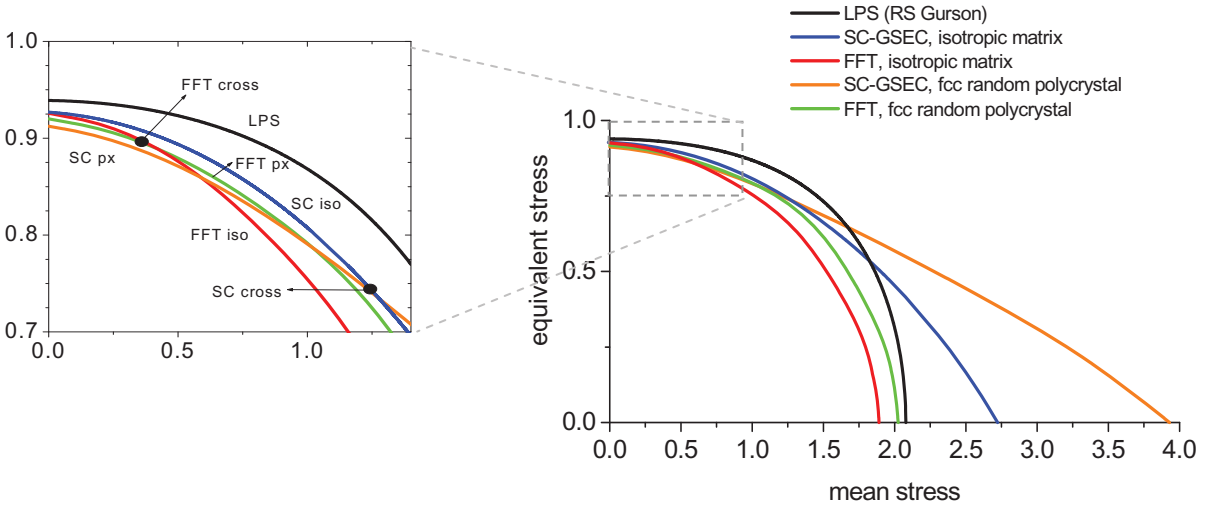

Fig. 1. Gauge surfaces corresponding to 5% porosity calculated by means of the full-field FFT-based method (red and green curves), and mean-field SC-GSEC estimates (blue and orange curves), for the cases of porous random fcc polycrystal (px) and porous material with uniform isotropic von Mises matrix (iso). LPS gauge surfaces also shown (black curves). Insert on the left shows a zoom in the low triaxiality region. Crossing points of the px and iso curves as predicted by FFT and SC-GSEC also shown.

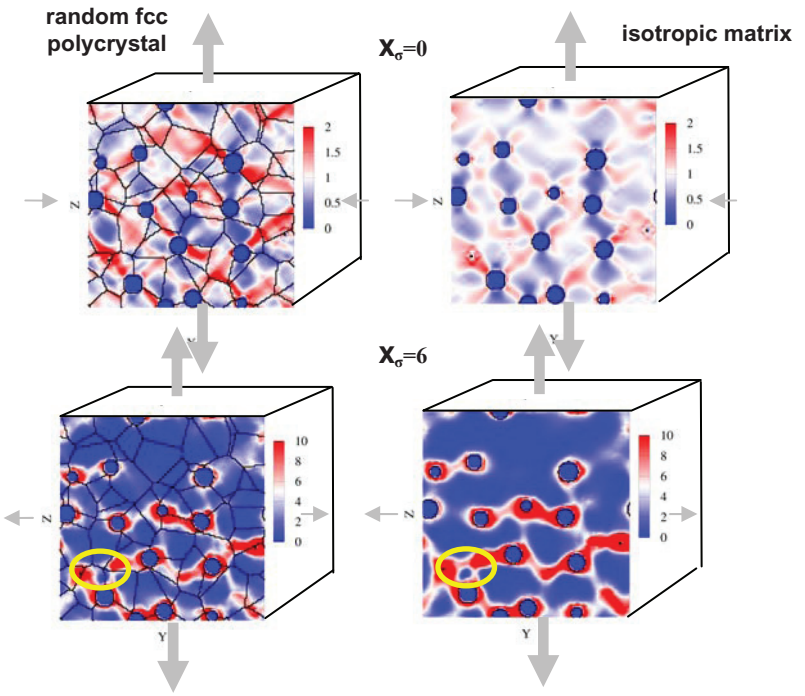

Fig. 2. Equivalent strain rate fields (normalized by the macroscopic equivalent strain rate) predicted with the FFT-based method, corresponding to the same 2-D section of the 3-D unit cells for the polycrystalline and von Mises voided solids, under macroscopic stress triaxialities of 0 and 6. The porosity level is 5%. The strain rate was nullified inside the cavities to improve visualization of the fields in the solid material. Thick arrows show the direction of the largest applied principal stress.

where the so-called gauge factor $\Lambda(\boldsymbol{\Sigma})$ is a homogeneous function of degree 1 in $\boldsymbol{\Sigma}$ and the $\boldsymbol{\Sigma}^* = \boldsymbol{\Sigma}/\Lambda(\boldsymbol{\Sigma})$ lies on the gauge surface (Eq. 56). Thus, we can determine the gauge surface by computing the effective stress potential for an applied macroscopic stresses of arbitrary magnitude, determining the corresponding gauge factor from (49), and rescaling the applied stress accordingly. Since our objective in to compare different predictions (e.g. FFT vs SC) for different porous material systems considered (e.g. polycrystals vs isotropic matrix), we will report gauge surfaces choosing the reference stress $\sigma_o = 2.574$, corresponding to the axisymmetric flow stress computed with FFT for the 200-grain unit-cell described earlier, representing the fully dense fcc polycrystal with isotropic crystallographic and morphological textures.

Figure 1 shows the 5% porosity gauge surfaces calculated by means of the full-field FFT-based method and the mean-field SC-GSEC estimates, for the cases of porous random fcc polycrystal (px) and porous material with uniform isotropic von Mises matrix (iso). Gauge surfaces predicted by means of Leblond-Perrin-Suquet's (LPS) [3] generalization of Gurson's theory to von Mises voided solids exhibiting power-law viscoplasticity are also shown. Fairly good agreement between the LPS Gurson-type predictions and the FFT simulations is observed, with the FFT results showing a somewhat softer response than the LPS model for the entire range of triaxialities. On the other hand, the comparison of the LPS and FFT gauge surfaces with those corresponding to SC-GSEC is good at low triaxialities, but the agreement deteriorates as the hydrostatic component becomes dominant, see below.

Concerning the effect of crystallinity, both the FFT and SC-GSEC models predict that the von Mises solid is softer than the polycrystalline solid under axisymmetric shear (stress-triaxiality $X_\sigma = 0$) but harder under hydrostatic tension. The crossing points between the FFT and SC-GSEC gauge functions corresponding to both types of solids can be appreciated in the insert in the left showing a zoom of the different curves for low triaxialities. This switch may be related to the role of crystal anisotropy on strain localization. Figure 2 shows FFT plots of equivalent strain rate, normalized by the macroscopic equivalent strain rate, in the polycrystalline and isotropic voided solids under macroscopic stress triaxialities $X_\sigma = 0$ and $X_\sigma = 6$. Note that, for each triaxiality, the scales are identical for both types of materials, but the maximum values of the strain rate field strongly increase at high triaxiality. At zero triaxiality, the strain rate is mildly localized in bands inclined with respect the direction of the largest principal stress. In both cases, these localization bands are formed due to interaction between neighboring voids, but in the case of the polycrystalline solid the bands are more intense when traversing soft grains. Thus, crystallinity seems to enhance localization at low triaxialities. As triaxiality increases, voids interact more strongly. In the case of high triaxiality, the strongest localization bands are formed in regions that are normal to the direction of the largest principal stress. However, in the polycrystalline solid, some of these bands are disrupted by the presence of hard grains and grain boundaries, see the locations marked with yellow ellipses in the plots for $X_\sigma = 6$, where the localization is appreciably lower in the polycrystal, compared with the same spot in the isotropic matrix solid. Our interpretation of these differences is that, at low triaxialities, when the hydrostatic component of the strain rate is small (or null) and the shear localization takes place mainly between voids that are close and favorably oriented with respect to each other, the statistically likely presence of at least one soft crystal orientation linking well-oriented voids should increase the strain localization, determining an overall softer behavior, compared to an isotropic matrix material with the same distribution of voids. On the other hand, at high triaxialities, when the expansion of the voids has to accommodate the dilatation applied to the aggregate, so that the material that surrounds the cavities undergo very large local deviatoric strains, the likely presence of at least one hard grain in the voids' surroundings seems to statistically disrupt the strain localization, leading to an overall harder response of the aggregate.

Concerning the comparison between FFT and SC-GSEC, while very accurate at low to moderate triaxialities, SC-GSEC estimates are seen to give overly hard predictions at larger triaxialities. In the hydrostatic point, these estimates are roughly twice as hard as the FFT results. Moreover, unlike the smooth FFT surfaces, they exhibit a corner at that point. As a result, SC-GSEC predictions for highly triaxial creeping processes will give unrealistically small hydrostatic strain rates and consequently will underestimate void growth at the initial stages of deformation. This problem of variational linear-comparison estimates is already well-known in the context of von Mises voided solids [37-38], as reflected by the corresponding curve (blue). Danas et al. [39] have proposed an ad-hoc remedy whereby the linearization scheme is forced to depend explicitly on the macroscopic stress triaxiality in such a way that the effective gauge surface tends to some specified hydrostatic point. In the case of von Mises solids, a suitable hydrostatic point is available from the well-known solution of a hollow sphere. A similar strategy could be envisaged for voided polycrystalline solids and will be explored in the future. In any event, as it stands, the SC-

GSEC theory proposed in this work should be accurate enough to model deformation processes involving low to moderate stress triaxialities.

5. Conclusions

We have carried out numerical simulations and theoretical calculations for the viscoplasticity of polycrystalline solids containing intergranular cavities. The simulations followed from a generalization to these materials of the FFT-based method, originally proposed by Suquet and coworkers and adapted to solid polycrystals by Lebensohn et al. The theoretical predictions, in turn, were obtained by means of suitable extension of the SC-GSEC formulation. In connection with the latter, we have presented a detailed description of the numerical aspects involved in the SC-GSEC implementation for voided polycrystals.

The simultaneous effects of porosity, crystallinity and crystallographic texture were investigated. Our findings seem to indicate that, at low triaxialities, the crystallinity of the matrix increases the strain localization due to the statistically likely presence of "soft links" (i.e. at least one soft crystal) in the surroundings of interacting voids, while the opposite happens for high triaxialities, i.e. the likely presence of at least one "hard" crystal in the vicinities of expanding cavities may disrupt strain localization.

Acknowledgements

RAL work supported by Joint DoD/DOE Munitions Technology Program and LANL LDRD-DR 2010026 Program. The work of MII and PPC was partially supported by LDRD-DR 2010026 through LANL subcontract number 84212-001-10.

References

[1] Lebensohn RA, Idiart M, Ponte Castañeda M, Vincent PG. Dilatational viscoplasticity of polycrystalline solids with intergranular cavities. *Phil. Mag.* 2011; **91**: 3038.
[2] Gurson AL. Continuum theory of ductile rupture by void nucleation and growth. *J. Eng. Mat. Tech.* 1977; **99**: 2.
[3] Leblond JB, Perrin G, Suquet P. Exact results and approximate models for porous viscoplastic solids. *Int. J. Plasticity* 1994; **10**: 213.
[4] Gologanu M, Leblond, Devaux J. Approximate models for ductile metals containing non-spherical voids–case of axisymmetric prolate ellipsoidal cavities. *J. Mech. Phys. Solids* 1993; **41**: 1723.
[5] Garajeu M, Michel JC, Suquet P. A micromechanical approach of damage in vicoplastic materials by evolution in size, shape and distribution of voids. *Comput. Meth. Appl. Mech. Eng.* 2000; **183**: 223.
[6] Benzerga AA, Besson J, Pineau A. Anisotropic ductile fracture Part II: theory. *Acta Mater.* 2004; **52**: 4639.
[7] Monchiet V, Cazacu O, Charkaluk E, Kondo D. Macroscopic yield criteria for plastic anisotropic materials containing spheroidal voids. *Int. J. Plasticity* 2008; **24**: 1158.
[8] Keralavarma SM, Benzerga AA. A constitutive model for plastically anisotropic solids with non-spherical voids *J. Mech. Phys. Solids* 2010; **58**: 874.
[9] Lebensohn RA, Liu Y, Ponte Castañeda P. Macroscopic properties and field fluctuations in model power-law polycrystals: full-field solutions versus self-consistent estimates. *Proc. Roy. Soc. Lond. A* 2004; **460**: 1381.
[10] Lebensohn RA, Liu Y, Ponte Castañeda P. On the accuracy of the self-consistent approximation for polycrystals: comparison with full-field numerical simulations. *Acta Mater.* 2004; **52**: 5347.
[11] Hill R. Continuum micro-mechanics of elastoplastic polycrystals. *J. Mech. Phys. Solids* 1965; **13**: 89.
[12] Hutchinson JW. Bounds and self-consistent estimates for creep of polycrystalline materials. *Proc. Roy. Soc. London A* 1976; **348**: 101.
[13] Molinari A, Canova GR, Ahzi S. Self consistent approach of the large deformation polycrystal viscoplasticity. *Acta Metall. Mater.* 1987; **35**: 2983.
[14] Lebensohn RA, Tomé CN. A study of stress state associated with twinning nucleation and propagation in anisotropic materials. *Acta Metall. Mater.* 1993; **41**: 2611.
[15] Masson R, Bornert M, Suquet P, Zaoui A. Affine formulation for the prediction of the effective properties of nonlinear composites and polycrystals. *J. Mech. Phys. Solids* 2000; **48**: 1203.
[16] Ponte Castañeda P. The effective mechanical properties of nonlinear isotropic composites. *J. Mech. Phys. Solids* 1991; **39**: 45.
[17] deBotton G, Ponte Castañeda P. Variational estimates for the creep behaviour of polycrystals *Proc. Roy. Soc. A* 1995; **448**: 121.
[18] Ponte Castañeda P, Nebozhyn M. Variational estimates of the self-consistent type for the effective behaviour of some model nonlinear polycrystals. *Proc. Roy. Soc. A* 1997; **453**: 2715.

[19] Idiart MI, Ponte Castañeda P. Variational linear comparison bounds for nonlinear composites with anisotropic phases. I. General results. *Proc. Roy. Soc. A* 2007; **463**: 907.
[20] Idiart MI Ponte Castañeda P. Variational linear comparison bounds for nonlinear composites with anisotropic phases. II. Crystalline materials. *Proc. Roy. Soc. A* 2007; **463**: 925.
[21] Ponte Castañeda P. Exact second-order estimates for the effective mechanical properties of nonlinear composites. *J. Mech. Phys. Solids* 1996; **44**: 827.
[22] Ponte Castañeda P, Willis JR. Variational second-order estimates for nonlinear composites. *Proc. Roy. Soc. A* 1999; **455**: 1799.
[23] Bornert M, Masson M, Ponte Castañeda P, Zaoui A. Second-order estimates for the effective behaviour of viscoplastic polycrystalline materials *J. Mech. Phys. Solids* 2001; **49**: 2737.
[24] Ponte Castañeda P. Second-order homogenization estimates for nonlinear composites incorporating field fluctuations: I- Theory. *J. Mech. Phys. Solids* 2002; **50**: 737
[25] Liu Y,Ponte Castañeda P. Second-order theory for the effective behavior and field fluctuations in viscoplastic polycrystals. *J. Mech. Phys. Solids* 2004; **52**: 467.
[26] Moulinec H, Suquet P. Numerical method for computing the overall response of nonlinear composites with complex microstructure. *Comput. Meth. Appl. Mech. Eng.* 1998; **157**: 69.
[27] Michel JC, Moulinec H, Suquet P. A computational method based on augmented Lagrangians and fast Fourier transforms for composites with high contrast. *Comput. Model. Eng. Sci.* 2000; **1**: 79.
[28] Lebensohn RA. N-site modelling of a 3-D viscoplastic polycrystal using Fast Fourier Transform. *Acta Mater.* 2001; **49**: 2723.
[29] Lebensohn RA, Brenner R, Castelnau O, Rollett AD. Orientation image-based micromechanical modelling of subgrain texture evolution in polycrystalline copper. *Acta Mater.* 2008; **56**: 3914.
[30] Lebensohn RA, Montagnat M, Mansuy P, Duval P, Meysonnier J, Philip A. Modeling viscoplastic behavior and heterogenous intracrystalline deformation of columnar ice polycrystals. *Acta Mater.* 2009; **57**: 1405.
[31] Laws N. On the thermostatics of composite materials. *J. Mech. Phys. Solids* 1973; **21**: 9.
[32] Willis JR. Variational and related methods for the overall properties of composites. *Adv. Appl. Mech*. 1981; **21**: 1.
[33] Lebensohn RA, Tomé CN, Ponte Castañeda P. Self-consistent modeling of the mechanical behavior of viscoplastic polycrystals incorporating intragranular field fluctuations. *Phil. Mag.* 2007; **87**: 4287.
[34] Lebensohn RA, Tomé CN, Maudlin PJ. A selfconsistent formulation for the prediction of the anisotropic behavior of viscoplastic polycrystals with voids. *J. Mech. Phys. Solids* 2004; **52**: 249.
[35] Michel JC, Moulinec H, Suquet P. A computational scheme for linear and non-linear composites with arbitrary phase contrast. *Int. J. Numer. Meth. Eng*. 2001, **52**: 139.
[36] Ponte Castañeda P, Suquet P. Nonlinear composites. *Adv. Appl. Mech.* 1998; **34**: 171.
[37] Pastor J, Ponte Castañeda P. Yield criteria for porous media in plane strain: second-order estimates versus numerical results. *C.R. Mécanique* 2002; **330**: 741.
[38] Bilger N, Auslender F, Bornert M, Masson R. New bounds and estimates for porous media with rigid perfectly plastic matrix. *C.R. Mécanique* 2002; **330**: 127.
[39] Danas K, Idiart MI, Ponte Castañeda P. A homogenization-based constitutive model for isotropic viscoplastic porous media *Int. J. Solids Struct.* 2008; **45**: 3392.

Appendix A. Calculation of second moments of the stress field in voided polycrystals

The average second moment of the stress field over a SR grain (r) of a voided thermoelastic polycrystal is given by Eq. (25):

$$\left\langle \boldsymbol{\sigma} \otimes \boldsymbol{\sigma} \right\rangle^{(r)} = \frac{1}{1-f} \frac{1}{c_g^{(r)}} \frac{\partial \tilde{u}_L}{\partial \mathbf{M}^{(r)}} \tag{A1}$$

Replacing Eq. (10) in (A1) we obtain:

$$\left\langle \boldsymbol{\sigma} \otimes \boldsymbol{\sigma} \right\rangle^{(r)} = \frac{1}{1-f} \frac{1}{c_g^{(r)}} \frac{\partial \tilde{\mathbf{M}}}{\partial \mathbf{M}^{(r)}} :: \left(\boldsymbol{\Sigma} \otimes \boldsymbol{\Sigma} \right) + \frac{1}{1-f} \frac{1}{c_g^{(r)}} \frac{\partial \tilde{\mathbf{e}}}{\partial \mathbf{M}^{(r)}} : \boldsymbol{\Sigma} + \frac{1}{1-f} \frac{1}{c_g^{(r)}} \frac{\partial \tilde{g}}{\partial \mathbf{M}^{(r)}} \tag{A2}$$

Using matrix notation for symmetric tensors, the first derivative in the right term can be obtained solving the following equation:

$$\Omega_{ijkl}\frac{\partial \tilde{M}_{kl}}{\partial M^{(r)}_{uv}} = \pi^{(r,uv)}_{ij} \tag{A3}$$

where i,j,k,l and u,v=1,6. The expressions for Ω_{ijkl} and $\pi^{(r,uv)}_{ij}$ are given below. Expression (A3) is a linear system of 36 equations with 36 unknowns (i.e. the components of $\partial\tilde{M}_{kl}/\partial M^{(r)}_{uv}$). In turn, the other two derivatives appearing in Eq. (A2) can be calculated as:

$$\frac{\partial \tilde{\dot{e}}_i}{\partial M^{(r)}_{uv}} = \zeta_{ikl}\frac{\partial \tilde{M}_{kl}}{\partial M^{(r)}_{uv}} + \kappa^{(r,uv)}_i \tag{A4}$$

$$\frac{\partial \tilde{g}}{\partial M^{(r)}_{uv}} = \varphi_{ij}\frac{\partial \tilde{M}_{ij}}{\partial M^{(r)}_{uv}} + \vartheta_i\frac{\partial \tilde{\dot{e}}_i}{\partial M^{(r)}_{uv}} + \eta^{(r,uv)} \tag{A5}$$

where ζ_{ikl}, φ_{ij}, ϑ_i, $\kappa^{(r,uv)}_i$ and $\eta^{(r,uv)}$ are given in below.

A.1. Calculation of $\partial B^{(r')}_{kj}/\partial M^{(r)}_{uv}$

From Eq. (14) we have (in matrix notation, all indices running from 1 to 6, except the phase indices (r) and (r')):

$$\frac{\partial B^{(r')}_{kj}}{\partial M^{(r)}_{uv}} = -\frac{1}{2}\left(\xi^{(r')}_{ku}B^{(r')}_{vj} + \xi^{(r')}_{kv}B^{(r')}_{uj}\right)\delta_{rr'} + \boldsymbol{\xi}^{(r')}\cdot\left[\frac{\partial \tilde{\mathbf{M}}^{*}}{\partial M^{(r)}_{uv}}\cdot\left(\mathbf{I}-\mathbf{B}^{(r')}\right) + \frac{\partial \tilde{\mathbf{M}}}{\partial M^{(r)}_{uv}}\right] \tag{A6}$$

where:

$$\boldsymbol{\xi}^{(r')} = \left(\mathbf{M}^{(r')} + \tilde{\mathbf{M}}\right)^{-1} \tag{A7}$$

In order not to clutter the notation, the first and second term on the right are written in explicit and implicit index notation, respectively. In the second term the indices (uv) (i.e.: the component of the local compliance with respect to which the derivatives are calculated) appear only to indicate such derivative, while in the first term they appear mixed with the indices that contract. In what follows, we will use this mix of explicit indices and implicit notation, when necessary for sake of clarity.

Deriving expression (16) we obtain:

$$\frac{\partial \tilde{M}^{*}_{ij}}{\partial M^{(r)}_{uv}} = \left(I-S\right)^{-1}_{ik}\frac{\partial S_{kl}}{\partial M^{(r)}_{uv}}\psi_{lj} + F^{S}_{ip}\frac{\partial \tilde{M}_{pj}}{\partial M^{(r)}_{uv}} \tag{A8}$$

where $\mathbf{F}^{S} = (\mathbf{I}-\mathbf{S})^{-1}\cdot\mathbf{S}$ and $\boldsymbol{\psi} = \mathbf{F}^{S}\cdot\tilde{\mathbf{M}}^{*} + \tilde{\mathbf{M}}^{*}$. Using the chain rule to express the first derivative on the right we can write:

$$\frac{\partial \tilde{M}^{*}_{ij}}{\partial M^{(r)}_{uv}} = \left(I-S\right)^{-1}_{ik}\frac{\partial S_{kl}}{\partial \tilde{M}_{pq}}\frac{\partial \tilde{M}_{pq}}{\partial M^{(r)}_{uv}}\psi_{lj} + F^{S}_{ip}\frac{\partial \tilde{M}_{pj}}{\partial M^{(r)}_{uv}} = \theta_{ijpq}\frac{\partial \tilde{M}_{pq}}{\partial M^{(r)}_{uv}} \tag{A9}$$

where:

$$\theta_{ijpq} = \left(I - S\right)^{-1}_{ik} \frac{\partial S_{kl}}{\partial \widetilde{M}_{pq}} \psi_{lj} + F^{S}_{ip}\, \delta_{jq} \tag{A10}$$

The algorithm for the calculation of $\partial \mathbf{S} / \partial \widetilde{\mathbf{M}}$ is given elsewhere [33]. Replacing (A8) in (A6) and after some manipulation we obtain:

$$\frac{\partial B^{(r')}_{kj}}{\partial M^{(r)}_{uv}} = -\frac{1}{2}\left(\xi^{(r')}_{ku} B^{(r')}_{vj} + \xi^{(r')}_{kv} B^{(r')}_{uj}\right)\delta_{rr'} + \xi^{(r')} \cdot \boldsymbol{\alpha}^{(r')} : \frac{\partial \widetilde{\mathbf{M}}}{\partial M^{(r)}_{uv}} \tag{A11}$$

where:

$$\alpha^{(r')}_{ijkl} = \theta_{imkl}\left(I - B^{(r')}\right)_{mj} + \delta_{ik}\delta_{jl} \tag{A12}$$

A.2. Calculation of $\partial \widetilde{M}_{ij} / \partial M^{(r)}_{uv}$

Deriving Eq. (20):

$$\frac{\partial \widetilde{M}_{ij}}{\partial M^{(r)}_{uv}} = \sum_{r'} \frac{c^{(r')}_{g}}{2}\left(\delta_{iu}\delta_{kv} + \delta_{iv}\delta_{ku}\right)\delta_{rr'}\, B^{(r')}_{kj} + \sum_{r'} c^{(r')}_{g} M^{(r')}_{ik} \frac{\partial B^{(r')}_{kj}}{\partial M^{(r)}_{uv}} + \frac{f}{1-f}\frac{\partial \widetilde{M}^{*}_{ij}}{\partial M^{(r)}_{uv}} \tag{A13}$$

Using (A8) and (A10) and calling $\boldsymbol{\beta}^{(r)} = \mathbf{M}^{(r)} \cdot \xi^{(r)}$ we get:

$$\begin{aligned} \frac{\partial \widetilde{M}_{ij}}{\partial M^{(r)}_{uv}} = \Bigg[& \frac{c^{(r)}_{g}}{2}\left(\delta_{iu} B^{(r)}_{vj} + \delta_{iv} B^{(r)}_{uj}\right) - \frac{c^{(r)}_{g}}{2}\left(\beta^{(r)}_{iu} B^{(r)}_{vj} + \beta^{(r)}_{iv} B^{(r)}_{uj}\right) + \\ & \left(\sum_{r'} c^{(r')}_{g} \boldsymbol{\beta}^{(r')} \cdot \boldsymbol{\alpha}^{(r')}\right) : \frac{\partial \widetilde{\mathbf{M}}}{\partial M^{(r)}_{uv}} \Bigg] + \frac{f}{1-f}\boldsymbol{\theta} : \frac{\partial \widetilde{\mathbf{M}}}{\partial M^{(r)}_{uv}} \end{aligned} \tag{A14}$$

From where:

$$\Omega_{ijkl} \frac{\partial \widetilde{M}_{kl}}{\partial M^{(r)}_{uv}} = \pi^{(r,uv)}_{ij} \tag{A15}$$

with:

$$\pi^{(r,uv)}_{ij} = \frac{c^{(r)}_{g}}{2}\left[\left(\delta_{iu} - \beta^{(r)}_{iu}\right) B^{(r)}_{vj} + \left(\delta_{iv} - \beta^{(r)}_{iv}\right) B^{(r)}_{uj}\right] \tag{A16}$$

$$\Omega_{ijkl} = \delta_{ik}\delta_{jl} - \sum_{r'} c^{(r')}_{g} \boldsymbol{\beta}^{(r')} \cdot \boldsymbol{\alpha}^{(r')} - \frac{f}{1-f}\boldsymbol{\theta} \tag{A17}$$

A.3. Calculation of $\partial \widetilde{\dot{e}}_{i} / \partial M^{(r)}_{uv}$

Deriving Eq. (21):

$$\frac{\partial \tilde{\dot{e}}_i}{\partial M_{uv}^{(r)}} = (1-f)\sum_{r'} c_g^{(r')} \dot{e}_k^{(r')} \frac{\partial B_{ki}^{(r')}}{\partial M_{uv}^{(r)}} \tag{A18}$$

Using (A11), we obtain:

$$\frac{\partial \tilde{\dot{e}}_i}{\partial M_{uv}^{(r)}} = \zeta_{ikl} \frac{\partial \tilde{M}_{kl}}{\partial M_{uv}^{(r)}} + \kappa_i^{(r,uv)} \tag{A19}$$

where:

$$\zeta_{ijk} = (1-f)\sum_{r'} c_g^{(r')} \dot{e}_m^{(r')} \xi_{ml}^{(r')} \alpha_{lijk}^{(r')} \tag{A20}$$

$$\kappa_i^{(r,uv)} = -(1-f)\frac{c_g^{(r)}}{2} \dot{e}_k^{(r)} \left(\xi_{ku}^{(r)} B_{vi}^{(r)} + \xi_{kv}^{(r)} B_{ui}^{(r)} \right) \tag{A21}$$

A.4. Calculation of $\partial \tilde{g} / \partial M_{uv}^{(r)}$

Deriving Eqs. (22) and (15):

$$\frac{\partial \tilde{g}}{\partial M_{uv}^{(r)}} = (1-f)\sum_{r'} c_g^{(r')} \dot{e}_i^{(r')} \frac{\partial b_i^{(r')}}{\partial M_{uv}^{(r)}} \tag{A22}$$

$$\frac{\partial b_i^{(r')}}{\partial M_{uv}^{(r)}} = -\frac{1}{2}\left(\xi_{iu}^{(r')} b_v^{(r')} + \xi_{iv}^{(r')} b_u^{(r')} \right)\delta_{rr'} - \boldsymbol{\xi}^{(r')} \cdot \frac{\partial \tilde{\mathbf{M}}}{\partial M_{uv}^{(r)}} \cdot \mathbf{b}^{(r')} + \boldsymbol{\xi}^{(r')} \cdot \frac{\partial \tilde{\dot{\mathbf{e}}}}{\partial M_{uv}^{(r)}} \tag{A23}$$

and replacing (A23) in (A22) and using (A9) we obtain:

$$\frac{\partial \tilde{g}}{\partial M_{uv}^{(r)}} = \varphi_{ij} \frac{\partial \tilde{M}_{ij}}{\partial M_{uv}^{(r)}} + \vartheta_i \frac{\partial \tilde{\dot{e}}_i}{\partial M_{uv}^{(r)}} + \eta^{(r,uv)} \tag{A24}$$

where:

$$\varphi_{ij} = -(1-f)\left[\sum_{r'} c_g^{(r')} \dot{e}_k^{(r')} \xi_{kl}^{(r')} \, b_p^{(r')} \right] \theta_{lpij} \tag{A25}$$

$$\vartheta_i = (1-f)\sum_{r'} c_g^{(r')} \dot{\varepsilon}_k^{(r')} \xi_{ki}^{(r')} \tag{A26}$$

$$\eta^{(r,uv)} = -(1-f)\frac{c_g^{(r)}}{2} \dot{\varepsilon}_i^{(r)} \left(\xi_{iu}^{(r)} b_v^{(r)} + \xi_{iv}^{(r)} b_u^{(r)} \right) \tag{A27}$$